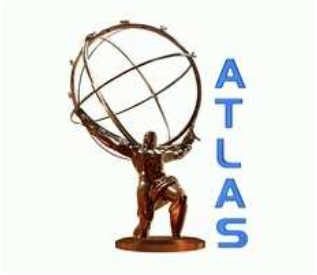

ATLAS NOTE

ATLAS-CONF-2012-022

March 4, 2012

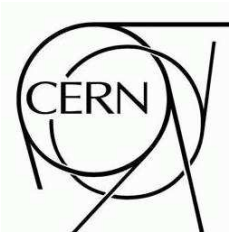

Search for charged long-lived heavy particles with the ATLAS Experiment at the LHC

The ATLAS Collaboration

Abstract

Several theories extending the Standard Model predict charged and heavy long-lived particles (LLP). Since LLPs potentially produced at the LHC can be slow, they could be identified through anomalous d$E/$dx energy loss measurement in the ATLAS Pixel detector. Selecting LLPs through the measurement of their track parameters in the vicinity of the interaction vertex gives access to various scenarios of new physics, including those where LLPs are metastable. A search for such particles with the ATLAS detector at the LHC is presented, based on a data sample corresponding to an integrated luminosity of about 2.1 fb^{-1}. No significant deviation from background expectations is observed, and therefore a cross section limit is set. With some model dependent assumptions, this can be interpreted as excluding gluino R-hadrons with masses smaller than 810 GeV.

1 Introduction

The discovery of exotic long-lived[1)] massive particles (LLPs) at the LHC would be of fundamental significance. Such searches are an important component of the early analysis of LHC experiments [1–3], as has been the case whenever a new collision energy has been reached [4–6]. The main motivation for LLP searches at the LHC arises from some proposed solutions to the gauge hierarchy problem [7, 8] which typically involve previously unseen particles at the TeV mass scale. In this work, new measurements from the ATLAS experiment on the production of LLPs are presented. Although the work is sensitive to many different models of new physics, results are presented in the context of Supersymmetry (SUSY) models predicting the existence of *R*-hadrons [9], which are heavy objects formed from a coloured sparticle (squark or gluino) and light SM quarks.

Earlier searches for *R*-hadrons at colliders were typically based on either the signature of a highly ionizing particle in an inner tracking system at LEP [10–12] or a slow-moving muon-like object at the Tevatron [13–17] and at the LHC [18]. The latter measurements rely on the assumption that the *R*-hadron is electrically charged in the muon spectrometer. However, hadronic scattering of *R*-hadrons in the dense calorimeter material in front of the muon detectors and the different mass hierarchy assumptions for the *R*-hadrons may increase the probability that the scattered *R*-hadrons are electrically neutral in the muon system. Such an effect is expected for *R*-hadrons formed from sbottom-like squarks [19]; the situation for gluino-based *R*-hadrons is unclear with several different models giving rise to different phenomenologies.

LLPs produced at the LHC are expected to be slow (β significantly below 1). The ATLAS detector [20] has a number of subsystems which provide information useful for discriminating LLPs from particles moving close to light speed. Two complementary subsystems are the Pixel detector [21], which provides measurements of ionization energy loss ($\mathrm{d}E/\mathrm{d}x$) and the Tile calorimeter (TileCal), which gives a direct measurement of the time-of-flight for particles traversing it. These two observables were used in the first ATLAS muon-agnostic search for LLPs [22]. The present work extends the search to about 2.1 fb^{-1} using the information of the tracker ($\mathrm{d}E/\mathrm{d}x$ from the Pixel detector and track parameter information from the whole Inner Detector) for the LLP identification. This is meant to extend the lifetime acceptance of LLPs and limit the model dependence on their interaction mechanism in the dense calorimeter material. It also extends the η acceptance ($|\eta| \leq 2.5$ for the tracker compared to 1.7 for the Tile calorimeter). A similar analysis strategy has been used by the CMS experiment [23].

This paper is organized as follows. Simulation of the signal is described before defining and justifying the event selection; detailed cut-flow tables for signal and data are built. The data-driven background estimation is then described in some detail. A careful discussion and evaluation of the systematic errors is then given. Finally, after a short description of the statistical method used to extract limits on *R*-hadron production cross sections and masses, results are shown.

2 Data set and Monte Carlo samples

2.1 Dataset

The analysis presented in this note is based on pp collision data at $\sqrt{s} = 7$ TeV recorded from March to August 2011. The corresponding integrated luminosity is 2.06 fb^{-1} after the data quality requirements are applied.

For this analysis events triggered by a calorimetric missing transverse energy ($E_{\mathrm{T}}^{\mathrm{miss}}$) exceeding 70 GeV are considered, as large $E_{\mathrm{T}}^{\mathrm{miss}}$ is a key identification variable for *R*-hadrons (see Section 4 for details).

[1)] The term long-lived is taken in this paper to mean that the particle has a decay length comparable to the size of the ATLAS silicon tracker (i.e. 60 cm in radius) or longer. No specific lifetime dependent study has been done in this paper, only stable LLP's have been considered.

2.2 Simulation of *R*-hadrons

A number of simulated signal samples are used in this analysis. As in [22], Monte Carlo simulations are used only to determine the efficiency of the *R*-hadron selection together with the associated systematic uncertainties. Predicted backgrounds are estimated using data, as described in Section 5.

Pair production of $\tilde{g}\tilde{g}$ is simulated in PYTHIA [24] using the DW tune [25, 26]. The string hadronisation model [27], incorporating specialised hadronisation routines [5] is used to produce final states containing *R*-hadrons. For gluino scenarios the probability for a gluino to form a gluon-gluino bound state, based on a colour octet model, is assumed to be 10% [5]. Results will be also reported considering a larger probabilty of 50%, although the signal efficiency dramatically decreases due to the larger presence of neutral *R*-hadrons in the final state.

The simulation of *R*-hadron interactions in matter is handled by dedicated GEANT4 routines [28, 29] based on three different models with differing assumptions.

The first model assumes that *R*-hadrons containing gluinos are simulated according to [19]. This model employs a triple-Regge formalism to describe hadronic scattering, and will henceforth be referred to as *Regge*.

The second physics model described in [30, 31] and hereafter referred to as *generic* has been used in other publications [32–34] and it imposes few constraints on allowed stable states. Doubly charged *R*-hadrons and a wide variety of "charge reversal" signatures in the detector are possible. Hadronic scattering is described through a purely phase space driven approach.

More recent models for the hadronic scattering of gluino *R*-hadrons predict that the majority of all produced *R*-hadrons will be electrically neutral after just a few hadronic interactions. The third model belongs to this family, is based on the bag-model calculations presented in [35] and is referred to as *intermediate*.

In the following, results are presented for the *generic* model. Efficiency variations resulting from these three models will be taken into account as systematic uncertainties.

The simulated samples have gluino masses in the range 200-1000 GeV, roughly matching the sensitivity that can be achieved given the statistical precision of the data sample on which the present analysis is based. The cross sections of the individual samples are normalised to the predictions of the PROSPINO NLO program [36] using CTEQ 6.6 parton density functions (PDFs) [37].

In all Monte Carlo samples, the primary collision event is overlaid with minimum bias simulated events to model the pile-up conditions in data.

3 Mass measurement with the Pixel Detector

The measurement of the ionization in the ATLAS Pixel detector [20] and its use for particle identification is described in detail in [38]. Below some significant information is summarized.

3.1 Specific energy loss from the Pixel detector

As the innermost sub-detector in ATLAS, the silicon Pixel detector provides at least three precision measurement points at radial distances from the LHC beam line r <13 cm for most tracks in the region $|\eta| < 2.5$. The sensors of the Pixel barrel (covering the central $|\eta|$-region) are placed on three concentric cylinders around the beam-line; the innermost layer (B-layer) is at a radius of 5 cm. The sensors of the end-cap (covering the high $|\eta|$-region) are located on three disks perpendicular to the beam axis on each side of the barrel. In the barrel(end-cap) the intrinsic accuracy is 10 μm in the $r-\phi$-plane and 115 μm in the $z(r)$-direction. The charge threshold is set to 3200$\pm$80 e^- throughout the $\sim$80 million pixels. Signals overcoming this threshold are time stamped within one beam crossing; the hit efficiency under these conditions exceeds 99%. When detector data is read out, the length of time for which the signal is above

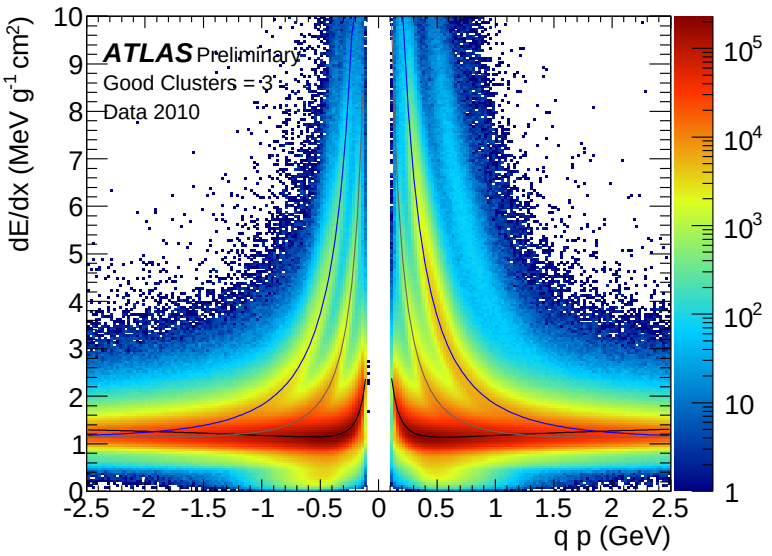

Figure 1: Distribution of dE/dx versus signed momentum for minimum bias collisions. In this data sample, from 2010 collisions, tracks are reconstructed down to 100 MeV p_{T}. The distribution of the most probable value for the fitted probability density functions of pions (black), kaons (gray) and protons (blue) are superimposed.

the threshold (ToT) is measured with 8 bit dynamic range. The maximum ToT value on a single pixel corresponds to 8.5 times the average charge released by a Minimum Ionizing Particle (MIP) moving perpendicular to the silicon detector If this value is exceeded, the ToT (and therefore the dE/dx) is not correctly measured: this sets the minimum measurable β with the dE/dx method.

The relation between ToT and the charge deposition in each pixel shows good linearity and stability as measured in devoted calibration scans, enabling an energy loss measurement for charged particles using the Pixel detector.

The charge released by a track crossing the Pixel detector is rarely contained within just one pixel. Neighbouring pixels are thus joined together to form clusters and the charge of a cluster is calculated by summing up the charges of all pixels after calibration correction. The specific energy loss, dE/dx is defined as an average of the individual cluster dE/dx measurements (charge collected in the cluster, corrected for the track length in the sensor), for the clusters associated with the track. To reduce the Landau tails, the average is evaluated after having removed the highest dE/dx cluster(s)[2)].

3.2 Mass reconstruction

Particles can then be identified by fitting each dE/dx and momentum measurement to an empirical Bethe-Bloch function and deducing their mass value. This particle identification method, described in detail in [38], uses a 5-parameter function to describe how the Most Probable Value of the specific energy loss ($\mathscr{M}_{\frac{\mathrm{d}E}{\mathrm{d}x}}$) depends on β:

$$\mathscr{M}_{\frac{\mathrm{d}E}{\mathrm{d}x}}(\beta) = \frac{p_1}{\beta^{p_3}} \ln(1 + (p_2\beta\gamma)^{p_5}) - p_4 \qquad (1)$$

[2)] The single highest dE/dx cluster is removed for tracks with 3 or 4 associated clusters, while for tracks having 5 or more clusters, the two highest dE/dx clusters are disregarded.

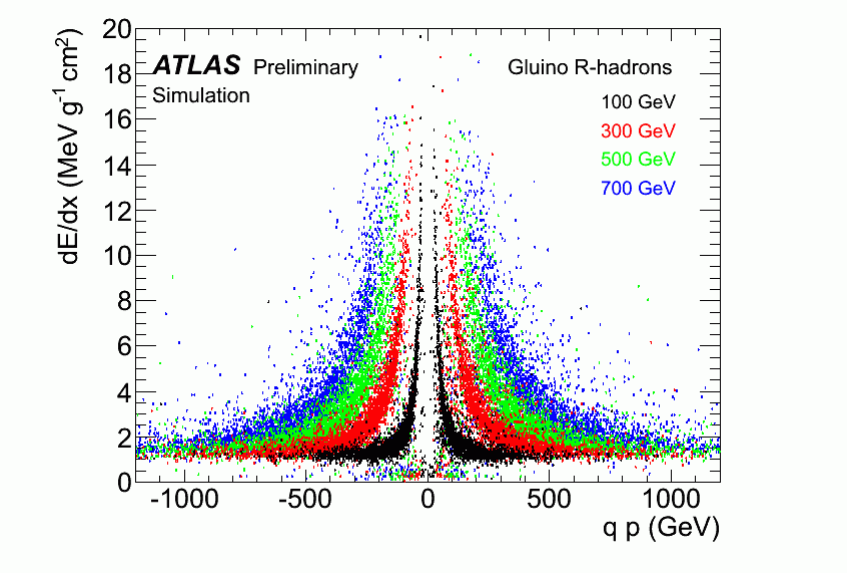

Figure 2: Simulated distribution of specific energy loss versus momentum for singly charged hypothetical *R*-hadrons of various masses.

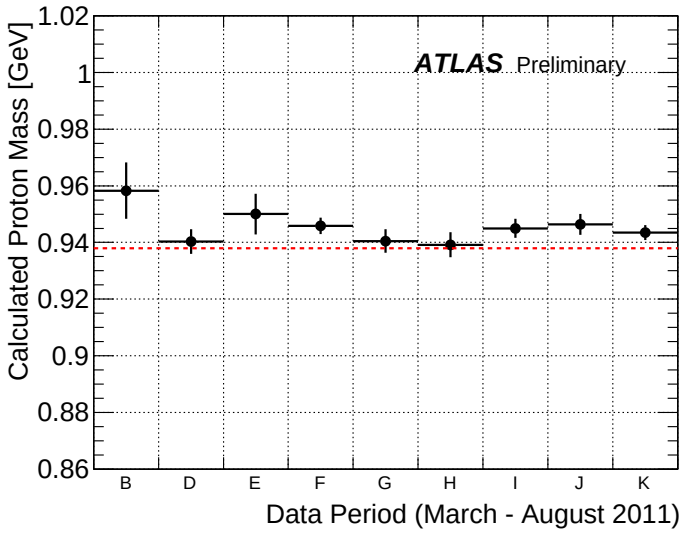

Figure 3: Proton mass calculated from the momentum measured in the Inner Detector and the specific energy loss measured in the Pixel detector. The data, covering the 2011 statistics considered for this analysis, are subdivided in periods of similar data taking conditions to illustrate the stability of the method. The red horizontal line represents the nominal proton mass value.

The 5 parameters used for the 2011 data are the same as those already used in the 2010 analysis, thus demonstrating the stability of the Pixel data. Fig. 1, taken from [38], shows how this function overlaps data for low momentum tracks. Fig. 2 shows the simulated Pixel $\mathrm{d}E/\mathrm{d}x$ spectra for singly charged hypothetical *R*-hadrons of masses 100, 300, 500 and 700 GeV. As expected, these distributions extend into the high Pixel $\mathrm{d}E/\mathrm{d}x$ region (Pixel $\mathrm{d}E/\mathrm{d}x \gg 1$ MIP) even for high momentum tracks. A MIP is expected to have an average $\mathrm{d}E/\mathrm{d}x$ of about 1.2 MeV/g cm^{-2} with a spread of $\sim$0.2 MeV/g cm^{-2} and a slight η dependence, increasing by $\sim$10% from central to high η. This is taken into account in the selection described in Section 4.2.

For all tracks having a reconstructed momentum p and a measured specific energy loss $\mathrm{d}E/\mathrm{d}x$ above the value for MIPs, a mass estimate M[3)] is obtained by inverting the fitted function $\mathscr{M}_{\frac{\mathrm{d}E}{\mathrm{d}x}}(\beta)$ (see Eq. 1), i.e. by numerically solving the equation $\mathscr{M}_{\frac{\mathrm{d}E}{\mathrm{d}x}}(p/M) = \mathrm{d}E/\mathrm{d}x$ for the unknown M.

The procedure is continuously monitored through precise measurement of the mass of known particles (kaons and protons) as illustrated in Fig. 3 and allows hypothetical heavy slow particles to be identified through their abnormal $\mathrm{d}E/\mathrm{d}x$ in a range of β of the order of 0.3-0.8 (see [38] and Section 4.2 for details). As already pointed out in [38], the mass resolution obtained with the $\mathrm{d}E/\mathrm{d}x$ method decreases with increasing mass values and the average mass estimate is systematically shifted to higher values by $\sim$ 8% (see Fig. 4). This is taken into account in the simulation and then in the limit setting.

4 Candidate selection

4.1 Trigger

The scope of the present study is to search for hypothetical *R*-hadrons selected through their high ionization close to the production point. At the trigger level this measurement is not available and other signatures must be used. To minimize the model-dependent biases, the strong nature of the gluino and squark production mechanisms and the associated QCD radiation is exploited. The "initial-state" radiation, especially from the gluon-gluon fusion (dominant production process for gluino masses lower than 600 GeV), gives rise to jets. The *R*-hadron is expected to deposit a small amount of energy in the calorimeter as it should behave like a MIP or even become neutral. The modest energy depositions of the heavy objects combined with the ISR jets naturally generates missing transverse energy. As the unprescaled jet triggers have a high threshold, it is preferable to trigger on the QCD radiation jets indirectly with an $E_{\mathrm{T}}^{\mathrm{miss}}$ trigger [39] ($E_{\mathrm{T}}^{\mathrm{miss}} >$70 GeV), which only relies on the energy deposited in the calorimeters.

The acceptance of this trigger is about 20% and slightly dependent on the mass of the R-hadrons as shown in Table 2.

4.2 Selection

This search is based on a sample of well-measured high-p_{T} tracks in events with large missing energy. The integrated luminosity analyzed is 2.06 fb^{-1}, corresponding to $\sim 1.2 \cdot 10^{14}\, pp$ inelastic collisions. Only 2.4 million events satisfy the calorimetric $E_{\mathrm{T}}^{\mathrm{miss}}$ trigger.

The selection starts with the confirmation of missing energy in the event, as the offline calculated $E_{\mathrm{T}}^{\mathrm{miss}}$ is measured more accurately than at the trigger level and it therefore provides the best background rejection. The offline calculated $E_{\mathrm{T}}^{\mathrm{miss}}$ [40] takes into account the dead material losses, the contribution from the identified muons and is calibrated at the correct energy scale. In the following, and if not otherwise specified, $E_{\mathrm{T}}^{\mathrm{miss}}$ will indicate this offline measurement.

[3)] Whenever $\mathrm{d}E/\mathrm{d}x < 1.26$ MeVg^{-1}cm^2 we assume that the measured $\mathrm{d}E/\mathrm{d}x$ is compatible with the value expected for a MIP and the mass estimate M is arbitrarily assigned a value $M = M_{\pi}$.

It is required to have $E_{\mathrm{T}}^{\mathrm{miss}}$ larger than 85 GeV, as this assures a good rejection of fake missing energy events while keeping most of the signal events independently of the pile-up conditions in data and of the *R*-hadron mass. Candidate events are required to have at least one primary vertex with a minimum of five tracks associated to it. At least one of the tracks in the event must have $p_{\mathrm{T}} > 50$ GeV with longitudinal and transverse impact parameters with respect to the reconstructed primary vertex lower than 1.5 mm. To assure good kinematic measurements, the high-p_{T} tracks are also required to be in the tracking system acceptance ($|\eta| \leq 2.5$), with at least three hits in the Pixel detector, of which at least one in the B-layer, and at least six hits in the silicon-strip based Semiconductor Tracker (SCT). The requirement of the minimum number of pixel hits also allows for a sufficiently precise measurement of the Pixel dE/dx. Three further cuts are required on the high-p_{T} and good quality primary tracks: in order to suppress backgrounds from jet production, the distance in $\eta - \phi$-space between the candidate and any other track with $p_{\mathrm{T}} \geq 5$ GeV must be greater than 0.25. The momentum p is required to be larger than 100 GeV, in order to significantly suppress backgrounds without any appreciable reduction of the signal in the interesting mass region. To have the signal-over-noise ratio constant over η the ionization dE/dx in the pixel clusters associated to the track must be larger than $p_0^{\mathrm{cut}} + p_1|\eta| + p_2\eta^2 + p_3|\eta|^3$ MeV/g cm^{-2}, where $p_0^{\mathrm{cut}}, p_1, p_2, p_3$ are set to 1.800, -0.045, 0.115, -0.033 respectively. With this request, the fraction of tracks exceeding the ionization limit is 1.6% independent on the pseudorapidity region.

Finally, in case of multiple tracks per event passing the isolation, high momentum and large ionization criteria, the one with the highest transverse momentum is selected as an *R*-hadron candidate to allow proper normalization.

Table 1: Observed event yields at different steps of the selection procedure. The total efficiency is computed with respect to the events that passed the trigger and the data quality decision. *Trigger* selects only those events which satisfy the calorimetric ($E_{\mathrm{T}}^{\mathrm{miss}} > 70$ GeV) online trigger. *Offline* $E_{\mathrm{T}}^{\mathrm{miss}}$ should exceed 85 GeV. *Primary vtx* requires a primary vertex with at least five tracks. Next cuts require in the event at least one track with: *High-*p_{T} corresponds to the request on high p_{T}, cuts on the impact parameters and Pixel/SCT clusters; *Isolation* refers to the requirement that the track satisfies $\Delta R_{\mathrm{track,othertrack}} > 0.25$ from any other track with $p_{\mathrm{T}} > 5$ GeV; *High-p* corresponds to the request on $p > 100$ GeV, *ionization* is the request on the Pixel dE/dx as explained in the text.

Cut level	**# Events**	**Cut Eff.**	**Total Eff.**
Trigger	2,413,863		
Offline $E_{\mathrm{T}}^{\mathrm{miss}}$	1,421,497	0.589	0.589
Primary vtx	1,368,821	0.963	0.567
High-p_{T}	212,464	0.155	0.0880
Isolation	32,188	0.151	0.0133
High-p	21,040	0.654	8.7E-03
ionization	333	0.016	1.4E-04

All requirements are summarized in the cut-flow chart in Table 1. Out of 2.06 fb^{-1}, 333 candidate events survive the selection cuts, none with more than one track passing all the selection criteria. Kinematical and geometrical properties of the candidate tracks at various stages of the selection are shown in Fig. 5.

The same selection is applied to the signal Monte Carlo samples. Table 2 shows the cut-flow for gluino *R*-hadrons samples of different masses. About 10% of the selected events have more than one track fulfilling the requirements on isolation and ionization. The overall signal efficiency varies from 6.7% for the lightest case shown in the table (400 GeV) to 8.4% for the heaviest (1000 GeV). The effect of the last cuts on the kinematical and geometrical properties of the tracks are shown in Fig. 6.

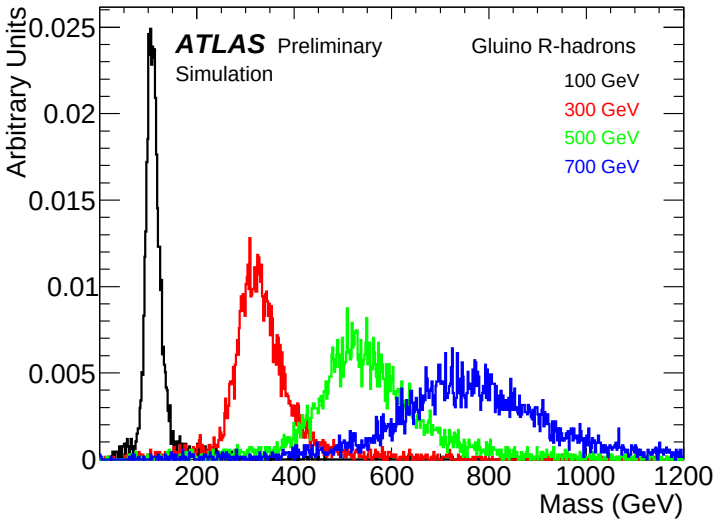

Figure 4: Distribution of the estimated mass obtained from momentum and specific energy loss measurement in the Pixel detector for simulated gluino R-hadrons of mass of 100, 300, 500 and 700 GeV.

Table 2: Expected efficiencies at different steps of the selection for signal Monte Carlo, based on the aforementioned gluino *R*-hadrons samples.

	Gluino 400 GeV		Gluino 700 GeV		Gluino 1000 GeV	
Cut level	**Cut Eff.**	**Total Eff.**	**Cut Eff.**	**Total Eff.**	**Cut Eff.**	**Total Eff.**
Trigger	0.205 ± 0.013	0.205 ± 0.013	0.219 ± 0.009	0.219 ± 0.009	0.177 ± 0.009	0.177 ± 0.009
Offline $E_{\mathrm{T}}^{\mathrm{miss}}$	0.98 ± 0.08	0.200 ± 0.013	0.99 ± 0.05	0.216 ± 0.009	0.98 ± 0.07	0.175 ± 0.009
Primary vtx	1.00 ± 0.09	0.200 ± 0.013	1.00 ± 0.05	0.216 ± 0.009	1.00 ± 0.07	0.175 ± 0.009
High-p_{T}	0.59 ± 0.06	0.120 ± 0.010	0.58 ± 0.04	0.129 ± 0.007	0.59 ± 0.05	0.108 ± 0.008
Isolation	0.84 ± 0.10	0.100 ± 0.009	0.84 ± 0.06	0.105 ± 0.006	0.88 ± 0.09	0.091 ± 0.007
High-p	0.99 ± 0.12	0.099 ± 0.009	0.99 ± 0.08	0.104 ± 0.006	1.00 ± 0.10	0.091 ± 0.007
Ionization	0.66 ± 0.09	0.067 ± 0.008	0.80 ± 0.07	0.085 ± 0.005	0.92 ± 0.09	0.084 ± 0.006

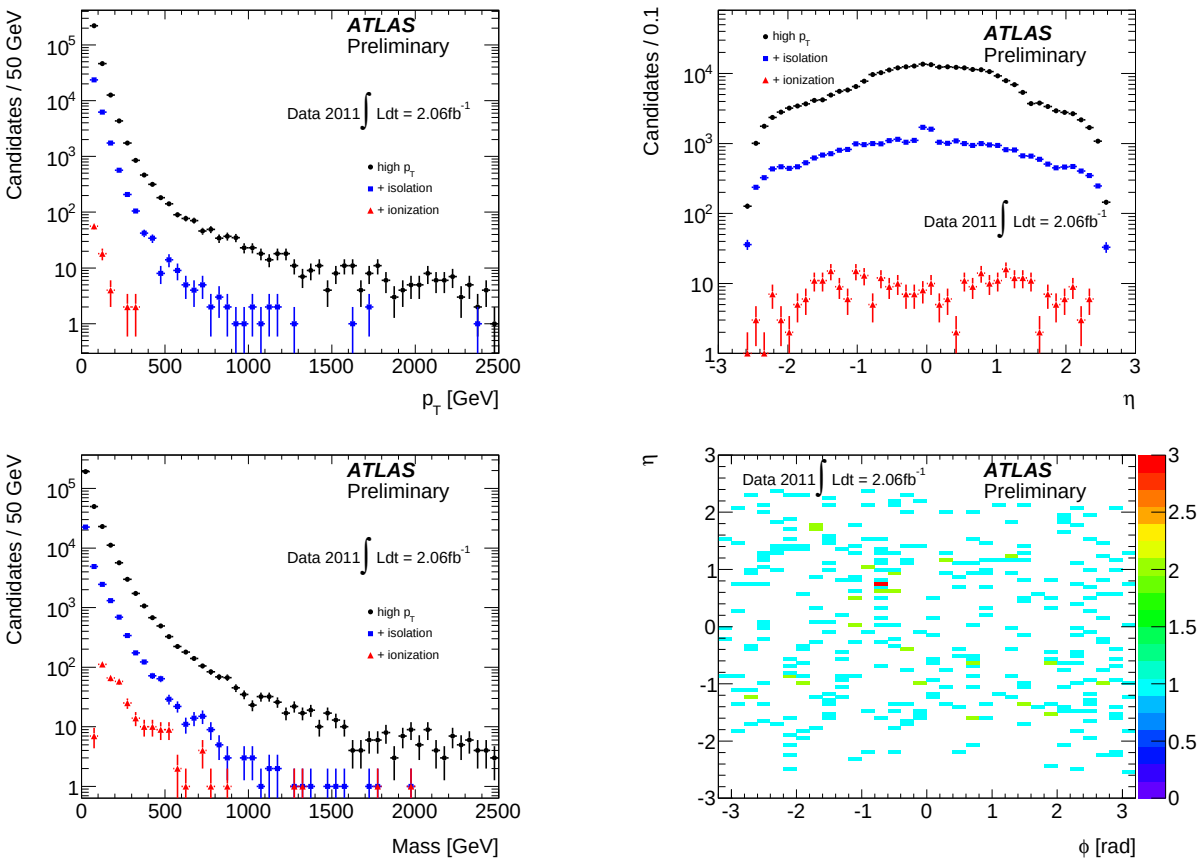

Figure 5: Distributions of p_{T}, η and mass for the data at the last steps of the applied selection. The peak at η=0 after the isolation cut in the top right plot is due to the limited acceptance of the muon spectrometer in this η-region. The bottom right plot shows the $\eta - \phi$ correlation of the selected 333 candidates.

5 Background estimation

To estimate the background a data-driven approach is used. The method consists of using the data sample to parameterize the key-variable distributions and their inter-dependence and then to generate a high-statistics random background sample based on these distributions. The choice of the control sample takes into account the non-negligible correlations between p, $\mathrm{d}E/\mathrm{d}x$ and η. The ionization dependence on the path length in the sensor is not linear [41], the pixel $\mathrm{d}E/\mathrm{d}x$ depends on η; the ionization also depends on the particle $\beta\gamma$ via the Bethe-Bloch formula and therefore on its momentum, until the Fermi plateau is reached; finally p and η are kinematically dependent.

Two background samples are used to describe the key-variables distribution. Both selections use the full data sample, but ensure that signal contamination is minimized.

- A first sample (Bkg1) is used to generate the η and p distributions and is selected according to the criteria described in Section 4.2 except the requirement on high ionization. Instead, to reduce the possible contribution of signal events in this background sample, a maximum limit on the $\mathrm{d}E/\mathrm{d}x$ (1.8 $\mathrm{MeVg^{-1}cm^2}$) is applied ensuring in this way orthogonality with the signal selection.

- A second background sample (Bkg2) is used to generate the $\mathrm{d}E/\mathrm{d}x$ templates. A background

sample free of signal but with no upper limits on the dE/dx is obtained by considering tracks that have a maximum momentum of 100 GeV. Specifically the background sample Bkg2 is selected as described in Section 4.2 with the same requirements on the tracks except that the requirement on the transverse momentum is looser, $p_T > 10$ GeV, and the momentum p is required to be between 20 and 100 GeV (where the Fermi plateau has already been reached).

Once the dependence of dE/dx, p and η have been obtained from the two background control samples, a high-statistics background sample consisting of two million p, η, dE/dx triplets is randomly generated according to the following procedure:

- First of all the momentum is generated according to a binned function based on Bkg1 events
- Then the pseudorapidity is generated according to the $\eta(p)$ binned functions based on Bkg1 events
- Finally the ionization is generated according to $dE/dx(\eta)$ binned functions based on Bkg2 events

The normalization of the generated background to the selected data is obtained by scaling the background to the data before the high dE/dx cut and in the shoulder region of the mass distribution where

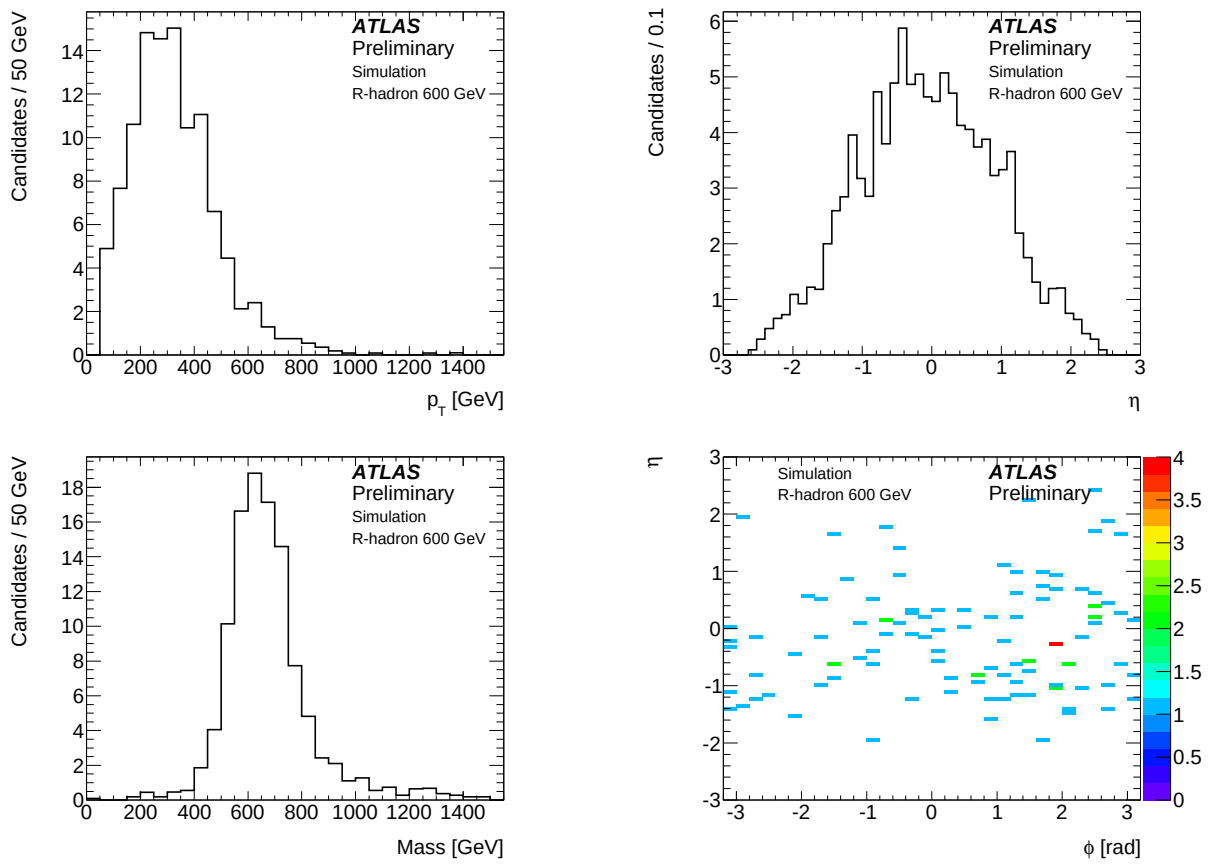

Figure 6: Distributions of p_T, η and Mass for a Monte Carlo sample (gluino *R*-hadrons 600 GeV) at the last step of the applied selection. The bottom right plot shows the $\eta - \phi$ correlation of the surviving events. The histograms are normalized to the number of events expected for an integrated luminosity of 2.06 fb^{-1} and a cross section of 0.634 pb.

no signal is expected (mass < 140 GeV). The systematic uncertainty associated with the background distribution is <10% and is discussed in detail in Sec. 6 while the statistical error is negligible and the normalization error is 0.8%. The number of expected background events at the end of the selection chain is 332.

6 Systematic uncertainties

In order to extract results on the production cross sections and the resulting *R*-hadron mass limits, several sources of systematic uncertainties are considered. In the following sections a list of systematic uncertainties together with a description of the methodology used to estimate their values are given. Since a data-driven approach is used to estimate the background contribution, the main systematics are broken down into uncertainties affecting the signal acceptance, the background estimation and all the other effects. Unless explicitly stated otherwise, the uncertainty is considered as a global factor. When mass-dependency is relevant, either we take into account the variation of uncertainty with mass or we conservatively take the largest value. An overview summary of the systematic uncertainties is shown in Table 3.

6.1 Uncertainties affecting the expected signal yield

6.1.1 Theoretical uncertainties

- LIMITED ACCURACY OF QCD CALCULATIONS TO MODEL THE PRODUCTION PROCESSES. The same systematic uncertainties as in the previous analysis [22] have been assumed, in particular the variation of the parton shower parameters in PYTHIA that can affect the total efficiency as they modify the phase space in which emissions can occur. These variations change the amount of *R*-hadrons passing the cuts, by up to 8.5%, with respect to the nominal setting.

- RATIO OF CHARGED *R*-HADRONS IN FINAL STATE. The ratios between events with 0, 1 or 2 charged *R*-hadrons in the final states have been varied by $\sim 3\%$, corresponding to $\pm$ 3 times the difference between the two generation models, PYTHIA and HERWIG. The main effect is observed on the efficiency to reconstruct a high-p_{T} track. The systematic uncertainty is evaluated as the difference in the total efficiency ($< 0.2\%$). It is not depending on the mass sample, therefore it is applied as a global uncertainty.

- SECONDARY SCATTERING OF *R*-HADRONS. A set of simulation samples based on different scattering models (so-called generic, Regge and intermediate) is available. The uncertainty is evaluated as the relative difference in efficiency with respect to the generic model; it does not depend on the mass value and its maximum value (11%) is applied as a global uncertainty.

6.1.2 Experimental uncertainties

- TRIGGER EFFICIENCY. The systematic uncertainty on the efficiency of the $E_{\mathrm{T}}^{\mathrm{miss}}$ online trigger used in this analysis has been evaluated by modifying the trigger turn-on curve. To perform this calculation the threshold and resolution parameters obtained from Monte Carlo have been varied within their fit uncertainties.

  To obtain a conservative estimate of possible turn-on discrepancies between real and simulated data, the parametrization obtained from simulated $W \to \mu\nu$ events is compared with the one measured on real W and Z candidates decaying to muons; the observed relative differences for the

threshold and resolution parameters are then applied to the simulated signal samples, obtaining corresponding efficiency systematic variations.

The fractional efficiency variations, corresponding to the individual systematic effects, are finally summed in quadrature and considered as overall trigger efficiency uncertainty; results are summarized in Table 3.

- $E_{\mathrm{T}}^{\mathrm{miss}}$ AND JET SCALE UNCERTAINTY. The effect on the total efficiency of the uncertainty on the jet energy scale and on the $E_{\mathrm{T}}^{\mathrm{miss}}$ measurement has been evaluated by applying a scale factor of $\pm$10% and a smearing of 20% to the $E_{\mathrm{T}}^{\mathrm{miss}}$ variable. These variations are in agreement with the analysis presented in [42]. Individual systematic effects are considered and the maximum of the fractional efficiency variations is taken as source of systematics. The result is asymmetric; the negative error depends on the mass ranging from -8.6% (200 GeV sample) to -3.4% (1000 GeV sample), while the positive error is always less than 1%.

- EFFECT OF PILE-UP. As the distribution of pile-up is different in data and Monte Carlo, signal efficiencies shown in Sec. 4.2 have been calculated reweighting the simulated samples to match the primary vertex distribution in data. The uncertainty in the reweighing procedure was evaluated by smearing the weighting factors: the effect turns out to be $< 2\%$ and not depending on the mass sample, therefore the maximum discrepancy is applied as a global uncertainty.

- DATA/MC PARAMETRIZATION OF THE PIXEL IONIZATION. An incorrect description of the particle energy loss in Monte Carlo samples could lead to an error in the signal efficiency. Comparisons between data and simulation have been performed for MIPs [38]. The Monte Carlo ionization is slightly larger, (Most Probable Value is 1.16 MeV g^{-1} cm^2 in MC, 1.12 in data) and the fraction of tracks with ionization larger than 1.8 MeV g^{-1} cm^2 is also slightly higher in Monte Carlo. To improve the description of the simulated ionization in the Pixel detector, a correction factor has been applied to the pixel $\mathrm{d}E/\mathrm{d}x$. The relative difference in the total efficiency depends on the R-hadron mass and varies from -8.9% (200 GeV sample) to -1.6% (1000 GeV sample).

- DATA/MC PARAMETRIZATION OF THE TRACK MOMENTUM. The track momentum is, with the ionization, an input variable for the mass estimation. Its imperfect description in simulation, mainly coming from alignment or material description, could bring to a difference in the signal efficiency. We assume the same uncertainty of 1% as in the previous analysis [22] in which a smearing function was applied to the track transverse momentum to account for differences between data and Monte Carlo.

- LAr INEFFICIENCY. About half of the statistics has been collected while a failure in the LAr calorimeter was affecting the region $\phi \times \eta$ = (-0.6,-0.8) $\times$ (0,1.4), corresponding to $\sim$1.5% of the Barrel LAr coverage. $E_{\mathrm{T}}^{\mathrm{miss}}$ in events with jets in that region can be mismeasured. As only part of the data and part of the acceptance are affected, a conservative uncertainty on the signal efficiency of 1% is considered.

6.2 Uncertainties on the data-driven background

As explained in Section 5, the background shape is generated according to binned histograms for p, $\eta(p)$ and $\mathrm{d}E/\mathrm{d}x(\eta)$ that reproduce these variable distributions and their inter-correlation. The generator sources have been obtained using control samples of background events. While the choice of the background samples reproduces well the candidates' properties, systematic uncertainties could come from the parametrization of the generator functions. The uncertainty is quoted as the maximum discrepancy, in the mass range under investigation, with respect to the nominal background.

- GENERATOR SYSTEMATICS. Two types of uncertainties have been studied: the effect of the binning changes for the template histograms and the use of functions instead of binned histograms as generators templates. Changing the binning of momentum and pseudorapidity distributions affects the Bkg1 generation and contributes <4% to the systematic error.

  The use of smoothed histograms instead of binned functions simultaneously for p, $\eta(p)$ and $\mathrm{d}E/\mathrm{d}x(\eta)$ results in a systematic uncertainty $<$ 3%. For the $\mathrm{d}E/\mathrm{d}x$ distribution, a further systematic uncertainty is obtained using an analytical function instead of the binned function. Two functions have been tested: a Crystal Ball over the full range or a Crystal Ball to describe the core and an exponential function to describe the tails of the distribution ($\mathrm{d}E/\mathrm{d}x > 2$ MeV g^{-1} cm^2). For both cases the systematic uncertainty is $<$ 3%.

- PILE-UP. The nominal background generation has been repeated subdividing the events according to the number of primary vertices, $\mathrm{n_{vtx}}$ that estimates the number of pile-up collisions in the same bunch-crossing. Three subsamples have been used: low ($\mathrm{n_{vtx}} \leq 6$), medium ($6 < \mathrm{n_{vtx}} \leq 8$), high pile-up ($\mathrm{n_{vtx}} > 8$). The overall effect is negligible ($<$ 2%).

The aforementioned sources of systematics result in an overall uncertainty $<$ 10%. This uncertainty, bin by bin, is the systematic error on the background distribution, shown in Fig. 7.

6.3 Uncertainties affecting the overall signal normalization

- LUMINOSITY. An uncertainty of 3.7% is used [43, 44].

- UNCERTAINTY ON THE SIGNAL PRODUCTION CROSS SECTION. The same systematic uncertainties as in the previous analysis [22] have been assumed:

  – The PROSPINO [45] next-to-leading order program is used to estimate the cross section for the pair production of gluinos. Variations of the renormalisation scale (chosen to be the gluino mass) up and down by a factor two lead to shifts in the cross section by up to $\sim$ 15%.

  – Variations due to the assumed parton density functions (PDFs) were also studied. Taking either CTEQ6.6 [37] or MSTW 2008 [46] changes the cross section by less than 5%.

7 Results

The mass distribution for the final sample, compared to the estimated background is shown in Fig. 7. No significant excess is observed. A frequentist scan of the signal confidence level with the CL_S method [47] is performed, as a function of the *R*-hadron cross section. The signal yield is smeared for the systematic uncertainties, as estimated in Section 6. The background distribution has errors combining statistical, normalization and systematic uncertainties, as explained in the previous section.

Limits on the cross section of the gluino *R*-hadrons are calculated at 95% of confidence level (CL) and are shown in Fig. 8 together with the predicted values for the cross section. The resulting limit on the gluino-based *R*-hadron mass is 810 GeV at 95% CL.

The main results are given in the hypothesis that the probability for a gluino to form a gluinoball is 10% [5]. The results obtained considering a probability of 50% (Fig. 8) indicate a limit on the gluino mass of $\sim$ 700 GeV at 95% CL.

Cross-checks of the upper limit estimate obtained using an alternative method (Barlow calculator, with Cousins and Highland priors [48]) give consistent results.

Table 3: Summary table for the systematic errors. If a range is reported, it indicates that the uncertainty depends on the mass sample. Either the edge values for a *R*-hadron mass of 200 GeV and 1000 GeV (systematic uncertainties on efficiency) or the minimum and maximum values (background) are quoted. If no range is reported, the systematic uncertainty is mass independent.

Systematic Uncertainties on Efficiency	[%]
QCD Accuracy	± 8.5
Ratio of charged *R*-hadrons	± 0.2
Scattering models	± 11
Trigger turn-on	$\pm 4 \div \pm 3$
MET scale	$-8.6 \div -3.4; +1$
Pile-up	± 2
Ionization Parametrization	$-9 \div -2$
Momentum Parametrization	± 1
LAr Inefficiency	± 1
Total uncertainty on Efficiency	$19 \div 14$
Systematic Uncertainties on Background	[%]
Binning p,η and $\eta(p)$	$-2 \div +4$
Smoothing	$-2 \div +3$
dE/dx CB	$-1 \div +3$
dE/dx CB+exp	$-1 \div +3$
Pile-up	$-2 \div +2$
Total uncertainty on Background	$1 \div 10$
Other uncertainties	
Luminosity	± 3.7
Prospino NLO	± 15
PDFs	± 5

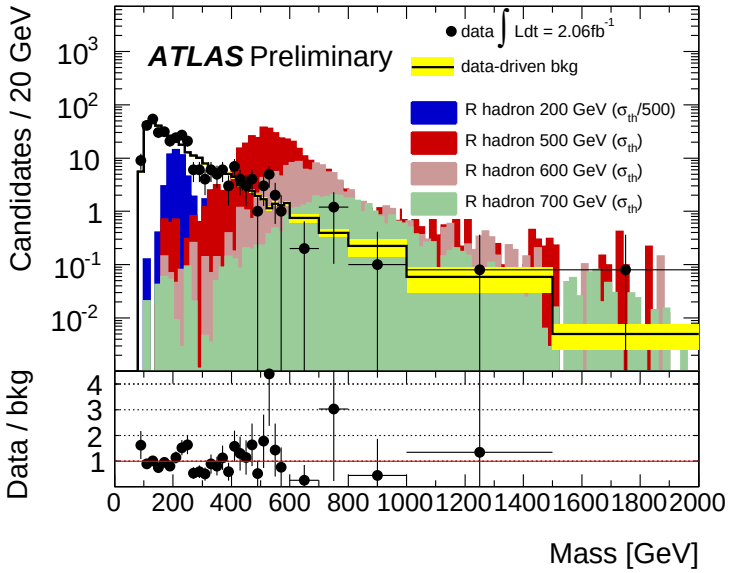

Figure 7: Mass distribution for data, background, and some expected simulated gluino *R*-hadron signals. The number of signal events is the one expected according either to the theoretical cross section (σ_{th}) or to a fraction of it, as specified. Below the plot, the ratio bin per bin between data and estimated background is given.

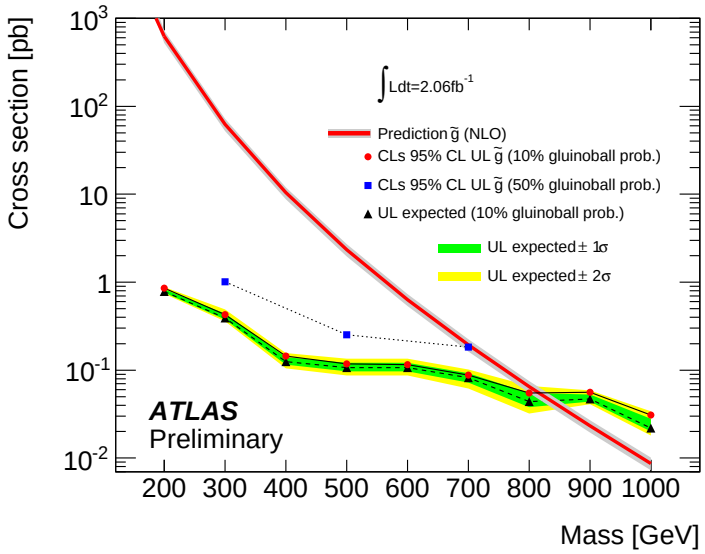

Figure 8: Cross section as a function of mass for gluino *R*-hadrons. Theoretical values for the cross section are shown with their error as a solid line, calculated 95% upper limits (UL) for a model considering a 10% (50%) gluinoball probability are given by points (squares). The expected upper limit in case of background only is also shown as triangles for a model considering a 10% gluinoball probability, with its $\pm 1,2\sigma$ bands.

8 Summary

A search has been made for gluino *R*-hadrons using the signature of specific ionization energy loss in the Pixel detector. No significant deviation from background expectations is observed, and therefore gluino R-hadrons with a mass smaller than 810 GeV are excluded at 95% confidence level.

References

[1] The ATLAS Collaboration, G. Aad et al., *Expected Performance of the ATLAS Experiment - Detector, Trigger and Physics*, CERN-OPEN-2008-020 (2009) .

[2] CMS Collaboration, *Search for Heavy Stable Charged Particles with 100 inverse picobarns and 1 inverse femtobarn in the CMS experiment*, CMS Analysis Note: PAS EXO-08-003 (2008) .

[3] The Moedal Collaboration, J. Pinfold et al., *Technical Design Report of the Moedal Experiment*, CERN-LHCC-2009-006 ; MOEDAL-TDR-001 (2009) .

[4] M. L. Perl, P. C. Kim, V. Halyo, E. R. Lee, I. T. Lee, et al., *The Search for stable, massive, elementary particles*, Int. J. Mod. Phys. **A16** (2001) 2137–2164.

[5] M. Fairbairn et al., *Stable massive particles at colliders*, Phys. Rept. **438** (2007) 1–63.

[6] A. R. Raklev, *Massive Metastable Charged (S)Particles at the LHC*, `arXiv:0908.0315`.

[7] L. Susskind, *The gauge hierarchy problem, technicolour, supersymmetry, and all that*, Phys. Rept. **104** (1984) 181–193.

[8] J. R. Ellis, *Perspectives in physics beyond the standard model*, . Sarajevo Summer School, Sarajevo, Bosnia-Herzegovina, 28 Sep -3 Oct 1998.

[9] G. R. Farrar and P. Fayet, *Phenomenology of the Production, Decay, and Detection of New Hadronic States Associated with Supersymmetry*, Phys. Lett. **B76** (1978) 575–579.

[10] DELPHI Collaboration, P. Abreu et al., *A Search for heavy stable and longlived squarks and sleptons in e^+ e^- collisions at energies from 130 GeV to 183GeV*, Phys. Lett. **B444** (1998) 491–502.

[11] ALEPH Collaboration, A. Heister et al., *Search for stable hadronizing squarks and gluinos in e^+ e^- collisions up to $\sqrt{s}$ = 209 GeV*, Eur. Phys. J. **C31** (2003) 327–342.

[12] DELPHI Collaboration, J. Abdallah et al., *Search for an LSP gluino at LEP with the DELPHI detector*, Eur. Phys. J. **C26** (2003) 505–525.

[13] CDF Collaboration, F. Abe et al., *Search for Heavy Stable Particles at the Fermilab Collider*, Phys. Rev. Lett. **63** (1989) 1447.

[14] CDF Collaboration, F. Abe et al., *Limits on the production of massive stable charged particles*, Phys. Rev. **D46** (1992) 1889–1894.

[15] CDF Collaboration, D. E. Acosta et al., *Search for long lived charged massive particles in anti-p p collisions at $\sqrt{s}$ = 1.8 TeV*, Phys. Rev. Lett. **90** (2003) 131801.

[16] D0 Collaboration, V. Abazov et al., *Search for Long-Lived Charged Massive Particles with the D0 Detector*, Phys.Rev.Lett. **102** (2009) 161802.

[17] CDF Collaboration, T. Aaltonen et al., *Search for Long-Lived Massive Charged Particles in 1.96-TeV p anti-p Collisions*, Phys. Rev. Lett. **103** (2009) 021802.

[18] ATLAS Collaboration, *Search for Heavy Long-Lived Charged Particles with the ATLAS Detector in pp Collisons at $\sqrt{s} = 7$ TeV*, Phys. Lett. **B703** (2011) 428–446.

[19] Y. R. de Boer, A. B. Kaidalov, D. A. Milstead, and O. I. Piskounova, *Interactions of Heavy Hadrons using Regge Phenomenology and the Quark Gluon String Model*, J. Phys. **G35** (2008) 075009.

[20] ATLAS Collaboration, *The ATLAS Experiment at the CERN Large Hadron Collider*, JINST **3** (2008) S08003.

[21] G. Aad et al., *ATLAS pixel detector electronics and sensors*, JINST **3** (2008) P07007.

[22] ATLAS Collaboration, *Search for Stable Hadronising Squarks and Gluinos at the ATLAS Experiment at the LHC*, Phys. Lett. B701 1-19 (2011) .

[23] CMS Collaboration, *Search for Heavy Stable Charged Particles*, CMS Analysis Note: PAS EXO-11-022 (2011) .

[24] T. Sjostrand, S. Mrenna, and P. Skands, *PYTHIA 6.4 Physics and Manual*, JHEP **05** (2006) 026.

[25] R. Field, *Tevatron Run 2 Monte-Carlo Tunes*, `arXiv:hep-ph/0610012`.

[26] T. Sjostrand and M. van Zijl, *A Multiple Interaction Model for the Event Structure in Hadron Collisions*, Phys. Rev. **D36** (1987) 2019.

[27] B. Andersson, G. Gustafson, G. Ingelman, and T. Sjostrand, *Parton Fragmentation and String Dynamics*, Phys. Rept. **97** (1983) 31–145.

[28] GEANT4 Collaboration, S. Agostinelli et al., *GEANT4: A simulation toolkit*, Nucl. Instrum. Meth. **A506** (2003) 250–303.

[29] ATLAS Collaboration, *The ATLAS Simulation Infrastructure*, Eur. Phys. J. **C70** (2010) 823–874.

[30] A. C. Kraan, *Interactions of heavy stable hadronizing particles*, Eur. Phys. J. **C37** (2004) 91–104.

[31] R. Mackeprang and A. Rizzi, *Interactions of coloured heavy stable particles in matter*, Eur. Phys. J. **C50** (2007) 353–362.

[32] A. C. Kraan, J. B. Hansen, and P. Nevski, *Discovery potential of R-hadrons with the ATLAS detector*, Eur. Phys. J. **C49** (2007) 623–640.

[33] CMS Collaboration, *Search for Stopped Gluinos in pp collisions at* $\sqrt{s} = 7$ TeV, Phys. Rev. Lett. **106** (2011) 011801.

[34] CMS Collaboration, *Search for Heavy Stable Charged Particles in pp collisions at* $\sqrt{s} = 7$ TeV, JHEP **3** (2011) 24.

[35] G. Farrar, R. Mackeprang, D. Milstead, and J. Roberts, *Limit on the mass of a long-lived or stable gluino*, JHEP **02** (2011) 18.

[36] W. Beenakker, R. Hopker, M. Spira, and P. M. Zerwas, *Squark and gluino production at hadron colliders*, Nucl. Phys. **B492** (1997) 51–103.

[37] P. M. Nadolsky, H.-L. Lai, Q.-H. Cao, J. Huston, J. Pumplin, et al., *Implications of CTEQ global analysis for collider observables*, Phys. Rev. **D78** (2008) 013004.

[38] ATLAS Collaboration, *dE/dx measurement in the ATLAS Pixel Detector and its use for particle identification*, ATLAS-CONF-2011-016 (2011) .

[39] D. Casadei et al., *The implementation of the ATLAS missing E_T triggers for the initial LHC operation*, ATL-DAQ-PUB-2011-001 (2011) .

[40] ATLAS Collaboration, *Performance of missing transverse momentum reconstruction in proton-proton collisions at $\sqrt{s}$ = 7 TeV with ATLAS*, Eur. Phys. J. **C72** (2012) 1844.

[41] H. Bichsel, *Straggling in thin silicon detectors*, Rev. Mod. Phys. **60** (1988) 663–699.

[42] ATLAS Collaboration, *Search for the Higgs boson in the H→ WW(*)→ lνlν decay channel in pp collisions at $\sqrt{s}$ = 7 TeV with the ATLAS detector*, `arXiv:1112.3832v1`. accepted for publication in PRL.

[43] ATLAS Collaboration, *Luminosity Determination in pp Collisions at s = 7 TeV using the ATLAS Detector at the LHC*, Eur. Phys. J. **C71** (2011) 1630.

[44] ATLAS Collaboration, *Luminosity Determination in pp Collisions at sqrt(s) = 7 TeV using the ATLAS Detector in 2011*, ATLAS-CONF-2011-116 (2011) .

[45] W. Beenakker, R. Hopker, and M. Spira, *PROSPINO: A Program for the production of supersymmetric particles in next-to-leading order QCD*, `hep-ph/9611232`.

[46] A. Martin, W. Stirling, R. Thorne, and G. Watt, *Parton distributions for the LHC*, Eur. Phys. J. **C63** (2009) 189–285.

[47] A. L. Read, *Presentation of search results: The CL(s) technique*, J. Phys. G **G28** (2002) 2693–2704.

[48] R. Barlow, *A Calculator for confidence intervals*, Comput. Phys. Commun. **149** (2002) 97–102.